

---

# Chemical waves in open flows of active media: Their relevance to axial segmentation in biology

---

Mads Kærn,<sup>\*a</sup> Michael Menzinger,<sup>a</sup> Razvan Satnoianu<sup>b</sup> and Axel Hunding<sup>c</sup>

<sup>a</sup> Department of Chemistry, University of Toronto, 80 St. George Street, Toronto, Ontario M5S 3H6, Canada

<sup>b</sup> Centre of Mathematical Biology, Mathematical Institute, Oxford University, 24–29 St. Giles, Oxford, UK OX1 3LB

<sup>c</sup> Department of Chemistry, H. C. Ørsted Institute, University of Copenhagen, Universitetsparken 5, Copenhagen DK-2100 Ø, Denmark

Received 10th April 2001

First published as an Advance Article on the web 12th November 2001

The boundary forcing of open flows of active media can lead to a variety of spatiotemporal structures, depending on the local kinetics of the medium and on the characteristics of the forcing. Here, we demonstrate that regardless of the local kinetics, the combination of flow and boundary forcing is a powerful method for replacing intrinsic modes with extrinsic ones. This entrainment of dynamics has important implications for biological morphogenesis. During early embryonic development it is frequently observed that stripes of gene expression and segments arise one after the other along a growth-axis. We show that axial growth can be viewed as an open flow of cells away from a growth zone. Based on this realisation, we demonstrate using three generic reaction–diffusion–advection schemes how a space-periodic structure is induced, one “segment” at a time along the growth/flow axis, by a segmental clock that is synchronised within the growth zone. The schemes are investigated in the context of an abrupt and a gradual change in the properties of the segmental clock. Experimental observations provide evidence that the latter is involved in the early development of many vertebrates.

---

## 1 Introduction

In past decades, pattern formation in far-from-equilibrium systems has been studied primarily in the context of reaction–diffusion systems with a rapidly diffusing inhibitor. The realisation<sup>1</sup> that the coupling of local kinetics to long-range inhibition may cause spontaneous symmetry-breaking has had a great impact on modern understanding of pattern formation.<sup>2–11</sup> On the other hand, symmetry breaking in open-flow reaction–diffusion–advection (RDA) systems has been considered only recently.<sup>12–22</sup>

The key element of an open flow<sup>12</sup> is that it begins at an upstream boundary where fresh medium is injected. This influx represents a boundary forcing that may entrain the temporally evolving medium into a variety of wave-patterns. The resulting spatio-temporal dynamics depends on the local kinetics of the medium (monostable, bistable, oscillatory) and on the character of the boundary forcing (constant, periodic, stochastic).

We argued recently<sup>21</sup> that axially growing embryos are actually equivalent to open flow systems: the movement of an organising centre or growth zone relative to the stationary cells is

equivalent to a relative flow of cells away from this upstream boundary. In this paper, we extend our earlier analysis<sup>22</sup> to open-flow RDA systems whose local kinetics is either monostable, bistable or oscillatory. The idea is that cell differentiation during early development is regulated, at least in part, by a space-period morphogen pattern imposed by the combination of a growth-induced flow and a periodic process, a segmental clock, at the growth/flow boundary. Our investigation is also relevant to pattern formation in periodically boundary-forced plug-flow reactors and in light-sensitive media whose properties change at a moving boundary of illumination.

The open flows investigated here are “plug-flows” modelled by the RDA equations of the type:

$$\frac{\partial \mathbf{u}}{\partial t} = \mathbf{f}(\mathbf{u}) - \phi \frac{\partial \mathbf{u}}{\partial x} + \mathbf{D} \frac{\partial^2 \mathbf{u}}{\partial x^2}, \quad \mathbf{u}(x=0, t) = \mathbf{b}(t), \quad (1)$$

where  $\mathbf{u}$  is a vector of interacting species,  $\mathbf{f}(\mathbf{u})$  describes their local interactions and  $\mathbf{D}$  is a diagonal matrix containing the diffusion coefficients. The flow coefficient,  $\phi$ , is equal for all the species. No-flux boundary conditions are imposed at the outflow,  $x = L$ , while  $\mathbf{b}(t)$  describes the characteristics of the temporal evolution at the inflow boundary,  $x = 0$ . The flow carries elements away from the boundary at velocity  $\phi$  and an element is located at  $x = a\phi$  after it has spent the time-period (or age)  $a$  in the flow.

In a chemical system, eqn. (1) describes an ideal plug-flow reactor illustrated in Fig. 1(a). In this context, Kuznetsov *et al.*<sup>14</sup> and later Andréßen *et al.*<sup>16</sup> studied eqn. (1) with oscillatory local kinetics, equal diffusion coefficients and constant boundary forcing. Based on linear analysis they predicted the formation of waves that are stationary relative to the inflow boundary. This finding was startling at that time since long-range inhibition is not involved. We have since confirmed their existence experimentally<sup>17</sup> and generalised the linear analysis.<sup>19</sup> We have also investigated periodic boundary forcing<sup>18</sup> which is of key relevance to biological morphogenesis.<sup>21,22</sup>

Space-periodic structure in the form of repetitive segments or bands of gene expression arises in many insects, worms and vertebrates one after the other along a growth-axis. A relevant case is the one where axial growth occurs by the divisions of stem cells at the tip of the growing embryo.

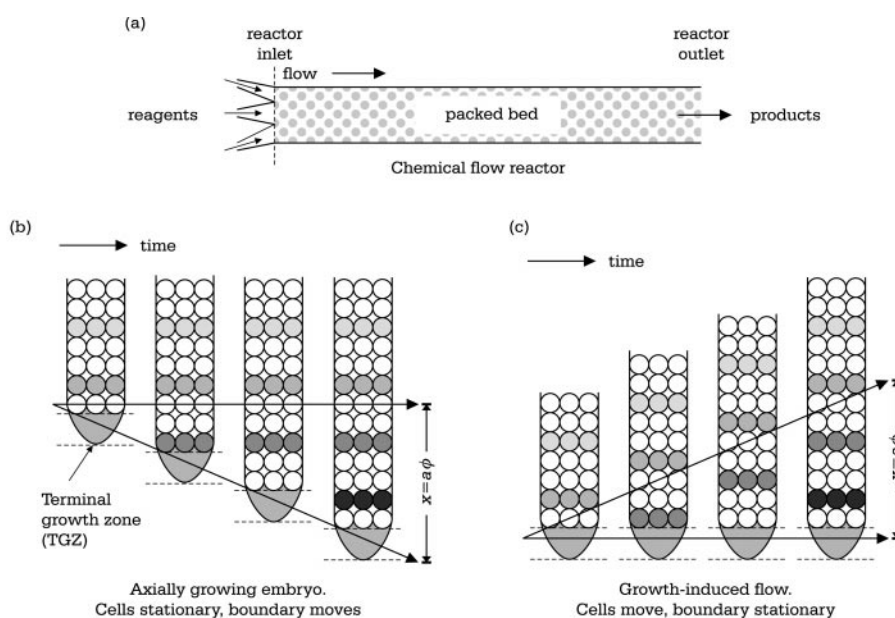


**Fig. 1** (a) Open flow packed-bed chemical reactor. Reagents are injected at one end and products removed at the other. The constant influx imposes a boundary forcing that may be constant, periodic or stochastic in time. (b) The typical reference frame of axially growing embryos. Daughter cells are stationary and the terminal growth zone is pushed downwards. (c) The growth zone is taken to be stationary. The continued shedding of progeny cells now amounts to a steady flow of cells away from the growth zone.

This is illustrated in Fig. 1(b). While the terminal growth zone (TGZ) of proliferating stem cells advances downward (slanted arrow), the daughter cells remain stationary with respect to their immediate environment and the embryo as a whole (horizontal arrow). Thus, the distance between the TGZ and the daughter cells increases as the embryo continues to grow.

Fig. 1(c) shows the same process in the reference frame where the TGZ is stationary (horizontal arrow). The continuous shedding of daughter cells from the TGZ now amounts to a steady flow of cells away from it (slanted arrow). As in the plug-flow described by eqn. (1), the distance between the TGZ and a cell with age  $a$  is given  $x = a\phi$  when the growth rate,  $\phi$ , is constant. The net result of a growth-induced flow is thus the same as in a flow system of the plug-flow type and axially growing biological systems can be approximated by eqn. (1) when cell–cell communication is modelled as a diffusion-like process.

As indicated by Fig. 1(b) and (c), there are two ways to model axial (*i.e.* anisotropic) growth. One is to keep the cells fixed while allowing the growth-boundary to move, as in Fig. 1(b). The flow is absent in this reference frame and the length of the system increases at a rate given by the growth velocity. The other is to keep the growth-boundary stationary and have cells move, as in Fig. 1(c). We have chosen to adapt this latter reference frame since the theory of open flow systems is well developed. Since we are modelling a growth-process, the boundary at  $x = L$  in eqn. (1) should strictly speaking move at a velocity given by  $\phi$ . However, the outflow boundary does not have significant influence on the dynamics of the system provided that its length is sufficiently large at all times. It suffices for the present purposes to have a constant value of  $L$ .

To induce cell differentiation, a space-periodic morphogen pattern must be stationary relative to individual cells, at least in the absence of a mechanism that can interpret a temporally varying morphogen level. The structures investigated throughout this paper are those that are stationary relative to cells and the developing embryo as a whole. Relative to the growth/flow boundary they have a velocity that is equal to the growth/flow velocity, *i.e.*  $c = \phi$ .

In a system described by eqn. (1), a structure that propagates with velocity  $c_0$  in the absence of a flow, will in the presence of a flow typically propagate with a velocity given by:

$$c^\pm = \phi \pm c_0. \quad (2)$$

The reaction–diffusion driven propagation is simply decreased when the structure moves against the flow ( $c^- < c_0$ ) and enhanced when it moves with the flow ( $c^+ > c_0$ ).

To obtain structures that move with velocity  $c = \phi$  relative to the upstream boundary it is required that  $c_0 = 0$ . Thus, we are looking for reaction–diffusion schemes that support stationary structures in the absence of a flow. They fall into three generic classes: (1) (nearly) stationary phase waves in media with oscillatory local kinetics, (2) media with steady or oscillatory local kinetics that support Turing structures and (3) media with bistable or excitable local kinetics that support stationary interfaces. When formed in the presence of a flow, we refer to them as flow-distributed structures (FDS).

The paper has two main sections. The idea pursued in Section 2 is that cells within the TGZ in Fig. 1(c) oscillate in synchrony and thereby impose a periodic forcing,  $\mathbf{b}(t) = \mathbf{b}(t + T')$ , on the shed daughter cells. We show how the periodic boundary forcing in the three generic scenarios may entrain the spatio-temporal dynamics and give rise to FDS with velocity  $c = \phi$ . In Section 3, we review the developmental process in vertebrates known as somitogenesis. Experiments have demonstrated that gene expression has wave-like character during somitogenesis in fish, birds and mammals and involves gene expression waves that propagate through the unsegmented tissue with decreasing width and velocity. Eventually, the velocity and wavelength coincides with what is predicted by each of the schemes investigated in Section 2. The spatio-temporal wave behaviour indicates that the local kinetics within cells change smoothly rather than abruptly, as assumed in Section 2. By allowing for a spatial variation of the kinetic parameters, we demonstrate that each of the three schemes account well for the observed wave behaviour.

## 2 Flow-distributed structures: general aspects

### 2.1 Phase-wave FDS

We first consider the spatio-temporal phase dynamics of a medium whose local kinetics supports an oscillation with period  $T_0$ . To derive the phase function,  $\theta(x, t)$ , *i.e.* how the oscillation phase

depends on space and time, we introduce a new space co-ordinate  $x/(\phi T_0)$ . This yields a new velocity  $\phi/(\phi T_0) = 1/T_0$ . Eqn. (1) is then re-scaled by introducing the co-ordinate  $z = x/(\phi T_0) - t/T_0$  that moves with the flow. In this reference frame, eqn. (1) transforms into:

$$\frac{\partial \mathbf{u}}{\partial t} = \mathbf{f}(\mathbf{u}) + \varepsilon \frac{\partial^2 \mathbf{u}}{\partial z^2} \equiv \mathbf{h}(\mathbf{u}, \varepsilon), \quad \text{with } \varepsilon = \frac{D}{\phi^2 T_0^2}, \quad (3)$$

The diffusion coefficients are set equal to  $D$  for all the species. The kinetics in the co-moving reference frame thus approaches that of the local kinetics as  $\varepsilon$  approaches zero,  $\mathbf{h}(\mathbf{u}, \varepsilon) \rightarrow \mathbf{f}(\mathbf{u})$  for  $\varepsilon \rightarrow 0$ . When  $\varepsilon = 0$ , diffusive interactions are non-existent and the cells oscillate independently of each other. This means that the time periodic solution of the local kinetics, *via* the above change of variables, translates to a space-periodic solution in eqn. (1). When diffusion cannot be ignored, but  $\varepsilon$  remains low,<sup>23</sup> it is reasonable to expect that cells oscillate with a period  $T$  such that  $T(\varepsilon) \rightarrow T_0$  for  $\varepsilon \rightarrow 0$ .

Suppose that the boundary forcing,  $\mathbf{b}(t)$ , has a period  $T'$  and that daughter cells (or volume elements) have oscillation phase  $\theta_0(\tau) = \tau/T'$  when they leave the growth zone (or reactor inlet) at  $x = 0$ . As a cell moves downstream, its oscillation phase advances linearly. After a time-period  $a$ , it is located at  $x = a\phi$  and the phase has advanced by  $a/T$ . Hence, the phase value at distance  $x$  and time  $t = a + \tau$  is given by the phase function:

$$\theta(x, t) = \theta_0(t - a) + \frac{a}{T} = \frac{t - a}{T'} + \frac{a}{T} = \frac{x}{\phi} \left( \frac{1}{T} - \frac{1}{T'} \right) + \frac{t}{T'}. \quad (4)$$

Differentiation of eqn. (4) with respect to  $t$  reveals that each fixed spatial point oscillates with the same period as the boundary  $T'$ . *The boundary forcing thus imposes itself onto the whole system.* The wavelength,  $\lambda$ , and the velocity,  $c$ , of the resulting phase waves are readily obtained from eqn. (4)<sup>21</sup> as:

$$c = \frac{-\phi}{R - 1}, \quad \lambda = \frac{\phi T'}{|R - 1|} \quad (5)$$

where  $R = T'/T$ . Phase dynamics, eqn. (5), thus predicts stationary waves,  $c = 0$ , for  $R = \infty$  (constant boundary forcing), upstream travelling waves,  $c < 0$ , for  $R > 1$ , homogeneous oscillations,  $c = \infty$ , for  $R = 1$  and downstream travelling waves,  $c > 0$ , for  $R < 1$ . The waves that are relevant here, *i.e.* those with  $c = \phi$ , are obtained when  $R = 0$ . This corresponds to the arrest,  $T \rightarrow \infty$ , of the intrinsic oscillation, for instance by the arrest of the local oscillators,  $T_0 \rightarrow \infty$ . The resulting phase-wave FDS has a wavelength that is given by  $\lambda = \phi T'$ .

Note that the diffusion term in eqn. (1) cannot be ignored when the local kinetics comes to a halt:  $\mathbf{f}(\mathbf{u}) \rightarrow 0$  for  $T_0 \rightarrow \infty$ . As a result, the FDS is a transient when formed for  $T_0 = \infty$ . Axial dispersion (diffusion) eventually homogenises the system and a non-uniform structure cannot be maintained. The phase-wave scenario is however still relevant for morphogenesis since the transient structure may be sufficiently long lived to induce cell differentiation. This will be discussed in Section 3.2. In addition, there are mechanisms other than setting  $T_0 = \infty$  that gives rise to an arrest of the intrinsic oscillation, *i.e.*  $T = \infty$ , as shown below.

## 2.2 Linear analysis

To investigate alternatives to the above phase-wave scheme, we now briefly discuss some useful insight provided by linear stability analysis. It predicts when a space-periodic sinusoidal perturbation, a mode, applied to a homogeneous state is amplified. To show that a linearly amplified mode gives rise to a persistent space-periodic structure requires a non-linear analysis and may involve secondary bifurcations from an already established pattern.<sup>24</sup> Such an analysis is beyond the scope of the present paper and will be pursued elsewhere. Despite these shortcomings, a linear analysis indicates when the relevant FDS may arise from an initially homogeneous state. Their amplification and stability are investigated by numerical simulations.<sup>25</sup>

We focus on systems with two interacting species, an activator  $u$  and an inhibitor  $v$ . The RDA

equations are:

$$\begin{aligned}\frac{\partial u}{\partial t} &= \gamma f(u, v) - \phi \frac{\partial u}{\partial x} + D_u \frac{\partial^2 u}{\partial x^2}, \\ \frac{\partial v}{\partial t} &= \gamma g(u, v) - \phi \frac{\partial v}{\partial x} + D_v \frac{\partial^2 v}{\partial x^2},\end{aligned}\quad (6)$$

where  $\gamma$  determines the time-scale of the kinetic terms  $f(u, v)$  and  $g(u, v)$ . The linear stability of a steady state  $(u_0, v_0)$  is determined by the temporal evolution of a small displacement  $U = u - u_0$  and  $V = v - v_0$  away from it. We look for solutions of the form:

$$U(x, t) = U_0 \exp^{\omega t + ikx}, \quad V(x, t) = V_0 \exp^{\omega t + ikx}, \quad (7)$$

where  $\omega$  determines the temporal evolution of the displacement,  $\text{Im}(\omega)$  determines the local frequency and  $k$  is the wavenumber.  $U_0$  and  $V_0$  are arbitrary constants.

A simplified description is obtained by expanding eqn. (6) in a Taylor series using eqn. (7) and keeping only the linear terms. Valid solutions to the resulting linear equations must satisfy a dispersion relation. It is given by:

$$\begin{aligned}2\omega &= \text{Tr} - k^2(D_v + D_u) - 2ik\phi \pm \sqrt{\Delta} \\ \Delta &= \text{Tr}^2 - 4 \det + 2k^2(D_v - D_u)(a_{11} - a_{22}) + k^4(D_v - D_u)^2,\end{aligned}\quad (8)$$

where  $\text{Tr} = a_{11} + a_{22}$ ,  $\det = a_{11}a_{22} - a_{12}a_{21}$  and  $a_{ij}$  are the elements of the Jacobian matrix at the steady state of the local kinetics.

The real part of  $\omega$ ,  $\text{Re}(\omega)$ , is independent of  $\phi$  since the wave number  $k$  is real and  $\phi$  only enters into eqn. (8) through the term  $ik\phi$ . Furthermore, the imaginary part of  $\omega$  is given by  $\text{Im}(\omega) = k\phi$  when the square root term in eqn. (8) is real (*i.e.* when  $\Delta > 0$ ). Since the phase velocity of a mode is given by  $c = \text{Im}(\omega)/k$ , the modes amplified have the desired velocity  $c = \phi$  when  $\Delta > 0$ .

To provide a specific example, we use a model of the FitzHugh–Nagumo (FHN) type.<sup>26,27</sup> It involves the kinetic terms:

$$f(u, v) = \varepsilon(u - u^3 - v), \quad g(u, v) = -v + \alpha u + \beta. \quad (9)$$

The parameters  $\varepsilon$ ,  $\alpha$  and  $\beta$  are associated with the time-scale separation between  $u$  and  $v$ , the coupling-strength of the inhibitor  $v$ , and the asymmetry of the phase plane structure, respectively. As shown in Fig. 2(a) the phase plane structure is symmetric for  $\beta = 0$  and the local kinetics has a steady state at the origin,  $(u_0, v_0) = (0, 0)$ . It is a focus for  $\alpha > 1$  and changes stability through a

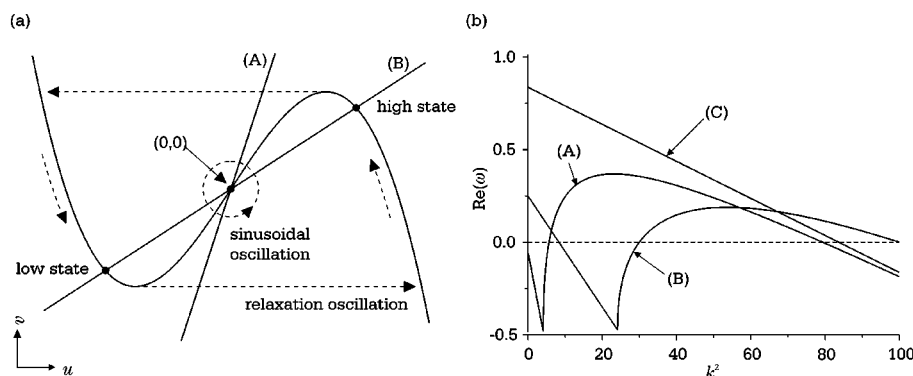


**Fig. 2** (a) Phase plane portrait of the FHN kinetics for  $\beta = 0$ . (A): The steady state at  $(0,0)$  is a focus for  $\alpha > 1$  and gives rise to relaxation oscillations for  $\varepsilon \gg 1$  and sinusoidal oscillations for  $\varepsilon > 1$ . The steady state is stable for  $\varepsilon < 1$ . (B): The steady state at  $(0,0)$  is a saddle point for  $\alpha < 1$ . Bistability is ensured when  $\alpha < 2/3$ . (b) The largest real part of the eigenvalues as a function of the wave number. (A): Local steady state is a stable focus ( $\varepsilon = 0.95$ ,  $\alpha = 2$ ,  $D_u = 0.01$ ,  $D_v = 0.1$ ). (B): Local steady state is an unstable focus ( $\varepsilon = 1.5$ ,  $\alpha = 2$ ,  $D_u = 0.01$ ,  $D_v = 0.1$ ). (C): Local steady state is a saddle point ( $\varepsilon = 1$ ,  $\alpha = 0.3$ ,  $D_u = D_v = 0.01$ ). Other parameter values are:  $\gamma = 1$ ,  $\beta = 0$ .

super-critical Hopf bifurcation when  $\varepsilon$  passes through a value of unity. It is stable for  $\varepsilon < 1$  and unstable for  $\varepsilon > 1$ . The steady state is a saddle point for  $\alpha < 1$  and bistability is ensured when  $\alpha < 2/3$  (for  $\beta = 0$ ). Excitability requires that  $\varepsilon$  and  $\beta$  be sufficiently large.

The dependence of  $\text{Re}(\omega)$  on  $k^2$  is illustrated in Fig. 2(b) for the cases where the local kinetics at  $(u_0, v_0) = (0, 0)$  is (A) a stable focus, (B) an unstable focus and (C) a saddle point. These three different cases are discussed below. The modes where  $\text{Re}(\omega[k^2])$  is positive are linearly unstable, meaning that a low amplitude spatial perturbation with wavelength  $\lambda = 2\pi/k$  is amplified.

### 2.3 Turing-type FDS

The steady state solution of the *local* kinetics is a stable focus when  $\text{Tr} < 0$  and  $\text{Tr}^2 - 4\text{det} < 0$ . The *homogeneous* steady state undergoes a Turing bifurcation when the inhibitor diffusion coefficient is increased relative to that of the activator and  $\Delta$  in eqn. (8) becomes positive. The onset of the Turing instability is unaffected by the flow (since  $\phi$  appears only in the imaginary part of  $\omega$ ) and the linearly unstable modes are the same as in the absence of a flow. The critical wavenumber,  $k_c$ , is given by:<sup>28</sup>

$$k_c^2 = \frac{a_{11}D_v + a_{22}D_u}{2D_uD_v} \quad (10)$$

and the limits of the range of unstable wave numbers,  $k \in [k_-; k_+]$ , are:

$$k_{\pm}^2 = k_c^2 \pm \frac{\sqrt{(a_{11}D_v + a_{22}D_u)^2 - 4D_uD_v \det}}{2D_uD_v}. \quad (11)$$

A perturbation with a wavenumber within this range may give rise to FDS with velocity  $c = \phi$  (since  $c = \text{Im}(\omega)/k$ ).

**2.3.1 Absolute and convective instability.** Before turning to the case of periodic boundary forcing, we briefly discuss some key general features of open flow systems using an open flow of Turing-unstable medium as example.

An open flow of a linearly unstable reaction–diffusion medium is either *absolutely* or *convectively* (spatially) unstable. If the flow velocity is low, a locally applied perturbation to the homogeneous state causes an inhomogeneity to develop and the edges of this structure spread both upstream and downstream. For equal flow coefficients, they have velocities given by eqn. (2) if they spread at velocity  $c_0$  in the absence of a flow. The system is said to be (linearly) *absolutely unstable* if  $c^- < 0$  and the slowest moving edge spreads upstream. In this case, the wavenumber and the velocity are selected intrinsically and they can be obtained from the dispersion relation (see *e.g.* ref. 29). An example of a Turing-type FDS formed under absolutely unstable conditions is shown in Fig. 3(a).

On the other hand, if the flow velocity is high and  $c^- > 0$ , both edges of the spreading structure are pushed downstream and eventually out of the system. As illustrated for the Turing-type FDS in Fig. 3(b), the initial perturbation is amplified only in the downstream direction. The system

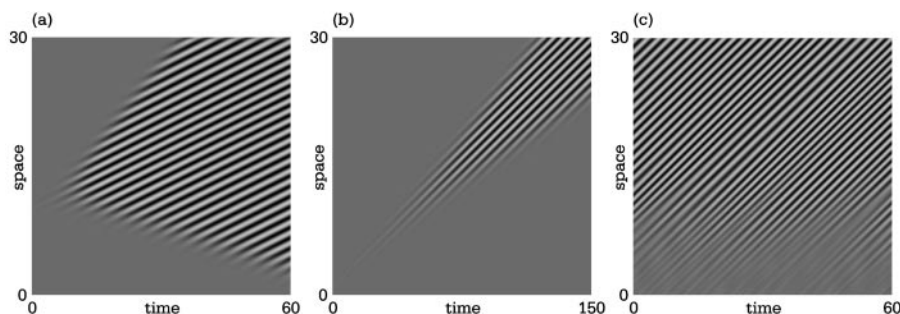


**Fig. 3** FDS of the Turing-type without periodic boundary forcing. (a) Absolutely unstable flow conditions for  $\phi = 0.1$ . (b) Convectively unstable flow conditions for  $\phi = 0.5$ . (c) Noise-sustained structures (see text). Parameter values used are:  $\gamma = 1$ ,  $\varepsilon = 0.95$ ,  $\alpha = 2$ ,  $\beta = 0$ ,  $D_u = 0.01$ ,  $D_v = 0.1$ . In (c), the time-step is 0.01 and the average distance between grid points is 0.05.

returns to the homogeneous state when the intrinsically selected spreading structure eventually is washed out. The system is now said to be *convectively unstable*.

A key feature of convectively unstable open flows is that they support *noise-sustained structures*.<sup>12</sup> They arise by the amplification of the small amplitude fluctuations that are present at all times in a real system. The fluctuations at the boundary are of key importance since they have the most time to grow. They can typically be decomposed into a spectrum of temporal frequencies,  $\omega'$ , which in the presence of a flow gives rise to a spectrum of spatial modes,  $k' = \phi\omega'$ . It is typically the one with the highest growth rate,  $\max(\text{Re}[\omega(k')])$ , that ultimately is selected. Fig. 3(c) shows a simulation of a noise-sustained Turing-type FDS. In the simulation, the boundary-value of activator is at each time-step set to a random value chosen from a normal distribution with standard deviation of 0.1.

The Turing-type FDS that arises at a low flow velocity (absolutely unstable conditions) or as a noise-sustained structure at high flow velocity (convectively unstable conditions) has the correct velocity,  $c = \phi$ . A traditional Turing mechanism with an intrinsically selected wavelength may thus be operational in axially growing systems. As we show next, the wavelength of the FDS may also be selected extrinsically. This is important in relation to fundamental biological problems such as size adaptation and regulation of developmental dynamics.

**2.3.2 Forced convective FDS.** The amplification of boundary-modes with wavelength  $\lambda = \phi T'$  allows for the entrainment of the spatio-temporal dynamics by applying a periodic boundary forcing with period  $T'$  (see *e.g.* ref. 20). It is required that the forcing amplitude is sufficiently higher than that of the background noise and that the imposed wavelength is within the appropriate range.

The space–time plots presented in Fig. 4 illustrate the effect of periodic boundary forcing on the spatio-temporal dynamics of a Turing unstable medium under convectively unstable flow conditions. The forcing mimics the Turing structure formed in the absence of a flow (not shown). The three simulations use the forcing periods: (a)  $T' = 2.1$ , (b)  $T' = 0.6$  and (c)  $T' = 3$ , all at  $\phi = 1$ . The wavelengths of the unstable modes lie between 0.70 and 2.6 for the chosen parameter values. The imposed periodicity is outside the range amplified by the medium in Fig. 4(b) ( $\lambda = 0.6$ ) and in Fig. 4(c) ( $\lambda = 3$ ).

In Fig. 4(a) the wavelength lies within the range supported by the medium and a new “segment” is added to the FDS each time an oscillation is completed at the boundary. The wavelength of the persistent Turing-type FDS is equal to 2.1, as expected. Other simulations have indicated that persistent structures with  $c = \phi$  exist for wavelengths  $\lambda = \phi T'$  within the spectrum of unstable modes.

Fig. 4(b) and (c) illustrate what may happen when the imposed wavelength lies outside the range supported by the medium. In Fig. 4(b) the imposed periodicity is too short and it decays to the homogeneous state. In Fig. 4(c) the imposed periodicity is too long. Now the amplitude of each

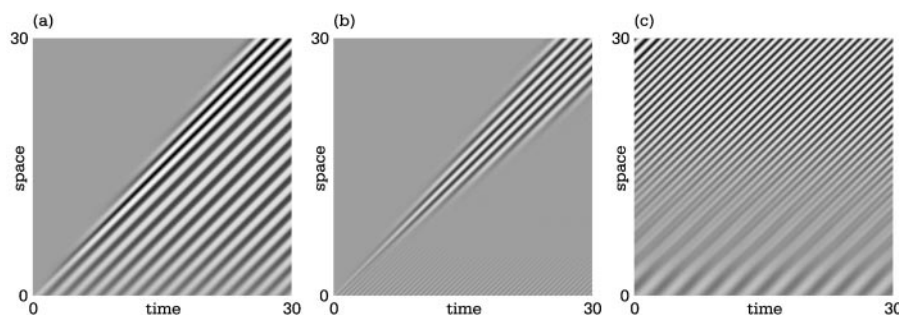


**Fig. 4** Forced Turing-type FDS. The boundary forcing is  $u(x = 0, t) = 0.2 \times \sin(2\pi t/T')$ ,  $v(x = 0, t) = 0.1 \sin(2\pi t/T')$  and  $\phi = 1$ . (a) The imposed periodicity,  $\lambda = \phi T'$ , is within the range of wavelengths supported by the medium ( $T' = 2.1$ ). (b) The imposed structure is too short ( $T' = 0.6$ ) and decays. (c) The imposed structure is too long ( $T' = 3$ ) and the decaying structure splits to give an FDS with a decreased wavelength. Parameter values are:  $\varepsilon = 0.9$ ,  $\alpha = 2$ ,  $\beta = 0$ ,  $\gamma = 1$ ,  $D_u = 0.01$ ,  $D_v = 0.2$ .

imposed segment initially decays before the segment splits into smaller ones. The wavelength is decreased and lies after the splitting within the range of wavelengths that are amplified.

Turing-type FDS with velocity  $c = \phi$  are also supported when the steady state of the local kinetics is an unstable focus. As shown in Fig. 2(b), the homogeneous steady state is in this case unstable to long-wavelength perturbations. The eigenvalues in eqn. (8) are complex conjugate at low values of  $k$  (since  $\Delta < 0$ ) and the structures that arise in this range do not have the relevant velocity (since  $\text{Im}(\omega) \neq \phi k$ ). However, as the wavenumber increases, the homogeneous state first becomes stable as  $\text{Tr} - k^2(D_v + D_u)$  becomes negative. As indicated in Fig. 2(b), it then becomes unstable (since  $\Delta(k^2)$  becomes positive). Unstable modes with  $\Delta(k^2) > 0$  have the relevant velocity (since  $\text{Im}(\omega) = \phi k$ ). Simulations have confirmed that these modes give persistent Turing-type FDS.

In summary, we have demonstrated that Turing-unstable media, be it with steady or oscillatory local kinetics, may give FDS with velocity  $c = \phi$  either under absolutely unstable conditions or under convectively unstable conditions. In the latter case, periodic boundary forcing may give rise to FDS that have the same properties as those predicted by phase dynamics for  $R = 0$ , namely velocity  $c = \phi$  and wavelength  $\lambda = \phi T'$ .

## 2.4 Interface-type FDS

The local kinetics of a bistable system typically supports two stable steady states that are separated in phase space by a saddle point. As shown in Fig. 2(b), a homogeneous system located at the saddle point has unstable modes with wavenumbers between  $k = 0$  and some upper critical value  $k_+$ . Hence, *any* imposed structure that has a wavelength longer than a critical value,  $\lambda_c$ , is initially amplified. From eqn. (8), the value of  $\lambda_c$  is obtained as:

$$\lambda_c^2 = 8\pi^2 D (\text{Tr} + \sqrt{\text{Tr}^2 - 4 \det})^{-1} \quad (12)$$

when  $D_u = D_v = D$ . The unstable modes all have the relevant velocity  $c = \text{Im}(\omega)/k = \phi$ , since  $\Delta(k^2) > 0$  for  $k < k_+$ . Which mode is ultimately selected depends, of course, on the nonlinear terms in the local kinetics.

Hagberg and Meron<sup>30</sup> did a detailed study of the bistable FHN kinetics in the absence of a flow. For  $\beta = 0$  and equal diffusion coefficients, there exists a stable stationary interface in a certain range of  $\varepsilon$ . This is exactly the case relevant here: a space-periodic interface-structure that is stationary in the absence of a flow is carried downstream at velocity  $c = \phi$  in the presence of a flow. When the diffusion coefficients are equal, a space-periodic interface-type FDS is supported when  $\varepsilon > 1$  and its wavelength is sufficiently long.<sup>31</sup>

In the presence of a flow, a boundary forcing that periodically switches between the two basins of attraction may give rise to a persistent FDS with wavelength  $\lambda = \phi T'$  and  $c = \phi$ . For this to occur, it is required that a critical nucleus<sup>32</sup> of each state is established at the boundary. An example of an appropriate forcing is one that is symmetric around the unstable steady state. In addition, the system must be nonlinearly convectively unstable<sup>33</sup> in order to avoid a competition between the boundary-mode and the intrinsically selected  $k = 0$  mode (*i.e.* one of the stable steady states). An example of a persistent FDS formed with equal diffusion coefficients is shown in Fig. 5(a).

In the absence of a flow, the stationary interface-solution is destroyed for  $\beta \neq 0$ .<sup>30</sup> The resulting spatio-temporal dynamics is illustrated in the space-time plot shown in Fig. 5(b). The parameters are the same as in Fig. 5(a) with the exception of an increased value of  $\beta$  (from zero to 0.1). It is observed that the spatial periodicity imposed by the boundary is initially amplified. However, an interface with  $c_0 = 0$  ( $c = \phi$ ) is not supported and the boundary-imposed FDS is only transient.

In the absence of a flow, increasing the diffusion coefficients makes stationary interfaces possible in the case where  $\beta \neq 0$ . Localised stationary structures with  $c_0 = 0$  maintained by rapid inhibitor diffusion have been studied intensively in both bistable and excitable reaction-diffusion media (see for instance ref. 27 and 31 and references therein). In the presence of a flow, a long-range inhibitor is required for persistent FDS with velocity  $c = \phi$  when the two steady states have different relative stability. An example of persistent interface FDS formed for  $\beta = 0.05$  is shown in Fig. 5(c).

Note, that excitable media support the same structures (*i.e.*  $c_0 = 0$ ) as do bistable media when the inhibitor diffusion coefficient is sufficiently large.<sup>31</sup> Simulations have confirmed that appropri-

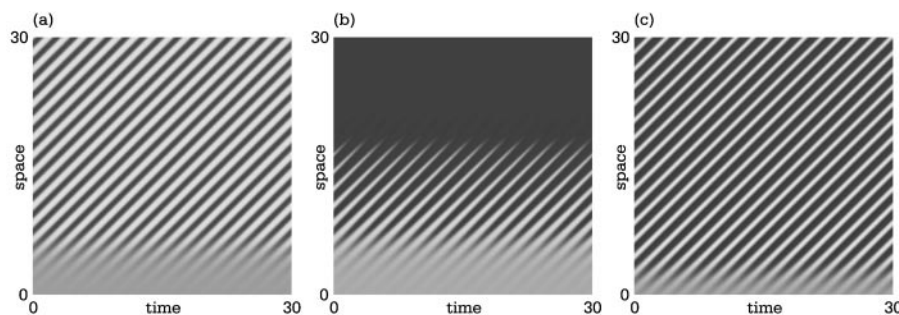


**Fig. 5** FDS of the interface-type. (a) The two stable steady states are equally stable ( $\beta = 0$ ). A persistent FDS with wavelength  $\lambda = \phi T'$  and  $c = \phi$  can be imposed by periodic boundary forcing ( $u(0, t) = 0.01 \sin(\pi t)$  and  $v(0, t) = 0$ ) with equal diffusion coefficients. (b) For  $\beta = 0.1$ , the more stable (dark) phase absorbs the less stable one ( $D_u = 0.01$ ,  $D_v = 0.05$ ). (c) The less stable phase (light) is stabilised when inhibitor diffusion is increased to  $D_v = 0.2$ . Forcing amplitude in  $u$  is 0.1 and  $\beta = 0.05$ . Other parameter values are:  $\varepsilon = 10$ ,  $\alpha = 0.3$ ,  $\phi = 0.5$ .

ate periodic boundary forcing and sufficiently rapid inhibitor diffusion can give rise to FDS with velocity  $c = \phi$  in both excitable media and in oscillatory media of the relaxation-type.

In summary, FDS with velocities  $c = \phi$  and wavelengths  $\lambda = \phi T'$  can arise robustly in periodically boundary-forced open flows. When the inhibitor diffusion is sufficiently rapid, they arise with mono-stable local kinetics (Turing unstable or excitable media), with bistable local kinetics or when the local kinetics supports oscillations. In addition, a long-range inhibitor is not strictly required: the transient phase waves that arise when  $T_0 \rightarrow \infty$  may be long-lived and persistent FDS arise when the local kinetics supports two steady states with the same relative stability.

### 3 Flow-distributed structures in biology

The most compelling experimental evidence for the operation of an FDS or FDS-like scheme is found during the vertebrate developmental process of somitogenesis. As shown below, the waves of gene expression observed during somitogenesis are not exactly of the type demonstrated in the previous section. The difference is that they have widths and velocities that change gradually as they propagate farther away from the growth zone. In this section, we show that the observed wave behaviour can be accounted for by either of the three generic schemes in Section 2, by allowing for a spatial variation of the kinetic parameters in eqn. (9).

#### 3.1 Somitogenesis

Somitogenesis is the process that establishes the blueprint of the vertebral column by the periodic formation of cell-clusters (the somites) along the body axis of the developing embryo. Fig. 6(a) shows a schematic drawing of a developing chick embryo. The structure at the top is the developing head and the spheres are the somites. The structure flanked by the somites is the neural tube (the precursor to the central nervous system). Structures that are repeated along the body axis, such as the vertebrae, ribs, skeletal muscles *etc.*, derive from the differentiated cells of the somites.

The somites on each side of the neural tube derive from rods of approximately cylindrical tissue called the presomitic mesoderm (PSM). The somites form by reorganisation of cells at the anterior (head-most) PSM boundary. As cells are removed from the anterior end of the PSM, new cells are continuously added to its posterior (tail-most) end and the length of the PSM remains relatively constant (10–12 somite-lengths in the chick). This axial growth (downward in Fig. 6) is required for continuous somite formation in many vertebrates<sup>34</sup> and seems to be facilitated, at least in part, by a stem-cell population residing in the tissue prior to the posterior PSM boundary.<sup>35,36</sup> The division of cells within the PSM seems mainly to increase its depth rather than its length or width.<sup>37</sup> For the present purpose, each PSM half is viewed as a rigid one-dimensional structure where non-differentiated cells enter at the posterior end and leave it at the anterior end.

The formation of somites at the anterior PSM boundary is preceded by intricate gene expression patterns believed to serve an important regulatory purpose (see ref. 22 for a discussion and

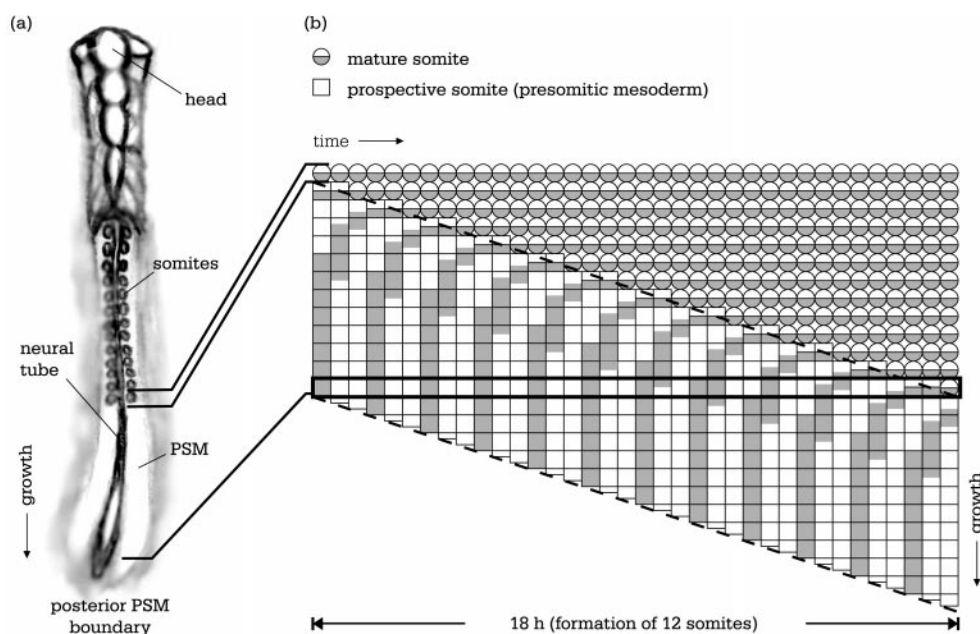


**Fig. 6** Somitogenesis in the chick. (a) Schematic drawing of the chick embryo. The spheres are the somites. (b) Spatio-temporal dynamics of gene expression waves during the formation of twelve somite pairs (adapted from ref. 36). Each vertical column represents a snap-shot taken at intervals of 30 min. Gray represents regions where *c-hairy1* mRNA is expressed. Somites are represented by circles and prospective somites within the PSM by squares. The anterior and posterior PSM boundaries are marked by slanted dashed lines. The solid horizontal box marks the position of a group of cells within the PSM. While it remains stationary with respect to the embryo, the movement of the PSM boundaries causes it to be transported across the entire length of the PSM during the 18 h period.

references). The spatio-temporal dynamics of *c-hairy1* mRNA expression in the chick embryo<sup>38</sup> is illustrated schematically in the space–time plot shown in Fig. 6(b). Regions where *c-hairy1* mRNA is expressed are marked in grey.

Fig. 6(b) illustrates the downward movement of the posterior and anterior PSM boundaries (marked by slanted dashed lines). Since cells remain fairly stationary relative to the embryo as a whole, the movement of the PSM boundaries is equivalent to a flow of cells through the PSM. The horizontal box outlines a group of cells (a prospective somite) that enters the PSM at its posterior end (at the left in Fig. 6(b)) and matures into a somite (circle) at the anterior end of the PSM (at the right in Fig. 6(b)). The net result of cells being stationary and boundaries that move is that this group of cells is transported across the entire length of the PSM over an 18 h time-period. Meanwhile, each cell completes about 10 expression cycles before the expression becomes constant near the anterior PSM boundary. At this point, the gene expression waves are stationary relative to cells and the wavelength of the gene expression pattern is one somite length  $l$ .

The operation of a cellular segmental clock<sup>39</sup> within the PSM indicates that the gene expression waves are phase waves, at least in the posterior-most part of the PSM. This is further substantiated by the observations<sup>38</sup> that they (1) are unaffected by transverse cuts through the PSM and (2) continue a predetermined program after small fragments of the PSM are separated from the rest of the embryo. In addition, cells enter the PSM with a periodically recurring phase of the gene expression cycle and are synchronised either before or while entering the PSM. It has been reported that the oscillation is present before the cells are added to the PSM.<sup>40,41</sup> The period of “boundary forcing” in the posterior region of the PSM is about 90 min in the chick.

We have demonstrated experimentally that the gene expression waves can be mimicked in an open flow of the oscillating ferroin-catalysed Belousov–Zhabotinsky reaction medium.<sup>21</sup> Blue bands were periodically initiated by a homogeneous oscillation near the reactor inlet and propagated downstream with a decreasing width and velocity, just like the bands in Fig. 6(b). This

spatio-temporal phase wave behaviour is the result of a gradually increasing intrinsic oscillation period as volume elements are carried away from the reactor inlet by the flow. Based on this scenario, we proposed in ref. 22 a simple phase model of somitogenesis where the period of the segmental clock gradually increases as cells move away from the posterior boundary. As a result, the value of  $R$  (see Section 2.1) decreases smoothly from a value of one at the posterior boundary to a value of zero at the anterior boundary, giving rise to a decreasing width and velocity of the phase waves.

While phase dynamics accounts for a large number of experimental observations,<sup>22</sup> the most compelling evidence for the involvement of an FDS or FDS-like mechanism is the experimentally observed wavelength within the array of mature somites. The length of the PSM is fairly constant and it grows by approximately one somite length,  $l$ , for each somite formed. A somite emerges every time a posterior oscillation cycle is completed and the velocity of the growth-induced flow is thus  $\phi = l/T'$ . With this flow velocity, the scenarios investigated in Section 2 all predict that the wavelength should be  $\lambda = \phi T' = l$ , exactly as observed. In the subsequent sections, we demonstrate that the three RDA schemes also account for the wave behaviour within the PSM when there is a gradual change in kinetic parameters.

### 3.2 RDA models of somitogenesis

In the RDA models of somitogenesis, we describe the segmental clock using FHN kinetics in eqn. (9) and the PSM by eqn. (6). No-flux boundary conditions are imposed at  $x = 0$ . This implies that the stem cells feeding the PSM are synchronised with the daughter cells just after the latter are formed. This is fully equivalent to having a periodic forcing with  $T' = T$  at the posterior PSM boundary.

The spatial variation of the oscillation period is obtained by introducing a third dynamic variable,  $w(a)$ , which, to preserve the kinematic nature of the regulation,<sup>22</sup> depends only on the time,  $a$ , a cell has spent in the PSM. The idea is that the properties of the segmental clock also change with cell age. A simple way to model the evolution of  $w$  is through a Fisher–Kolmogorov type logistic equation:<sup>42</sup>

$$\frac{dw}{da} = \varepsilon_w w(1 - w^p), \quad (13)$$

where  $a$  is the age of a cell. This is equivalent to a scenario where a factor, such as a protein or DNA transcription factor, is present in low levels within the stem-cell population and its starts to accumulate when cells enter the PSM.

The solution of eqn. (10) is for  $p = 1$  given by:

$$w(a) = \frac{w_0 \exp(\varepsilon_w a)}{1 - w_0 + w_0 \exp(\varepsilon_w a)}. \quad (14)$$

where  $0 < w_0 \ll 1$  is the level of  $w$  when a cell enters the PSM. It is a relatively steep saturation curve that connects the initial value  $w(0) = w_0$  to the steady state at  $w = 1$  for large  $a$ . Nonlinear response functions with a shape similar to that of eqn. (11) are frequently found in covalent modification cascades, genetic regulation and signalling pathways (see *e.g.* ref. 43). For the present purposes, a more elaborate model of the regulatory network is not required.

Our investigation is intended to demonstrate that each of the three generic FDS scenarios, in principle, may be operational in somitogenesis. Very little is known about the kinetics of the segmental clock, its spatio-temporal regulation or the role of cell–cell communication. We have not attempted to fit the model parameters to experimental observations and have only considered the simplest couplings. An overview of the different scenarios investigated is given in Table 1.

In the reference frame where the posterior PSM boundary is stationary, eqn. (10) is modelled by the RDA equation:

$$\frac{\partial w}{\partial t} = \varepsilon_w w(1 - w^p) - \phi \frac{\partial w}{\partial x} + D_w \frac{\partial^2 w}{\partial x^2}. \quad (15)$$

A non-uniform spatial profile,  $w(x)$ , arises along the length of the PSM when  $w$  is kept at a constant value  $w_0$  at  $x = 0$ . While  $w$  is intended to be strictly cell intrinsic, a small diffusive term,

**Table 1** Summary of FDS scenarios investigated and the couplings used.  $T_0$  is the oscillation period of the local FHN kinetics for  $w = 0$  and  $\delta$  is a constant

Section and scenario	Coupling	Effect on kinetics
3.2 Phase-wave FDS	$\gamma(a) = T_0[1 - w(a)]$	Arrest of oscillation
3.3 Turing-type FDS	$\varepsilon(a) = (\varepsilon_0 - \delta)[1 - w(a)] + \delta$ $\gamma(a) = T_0[1 - \delta w(a)]$	Oscillatory to mono-stable or slowing down of oscillation
3.4 Interface-type FDS	$\alpha(a) = \alpha_0[1 - \delta w(a)]$	Oscillatory to bistable

$D_w$ , is needed to avoid numerical instabilities in the simulations. The deviation between the solution of eqn. (12) and eqn. (11) (with  $a = x/\phi$ ) is however inconsequential when  $D_w \leq 0.01$ . Note that the case of periodic boundary forcing is recovered when  $w$  changes abruptly from zero at  $x = 0$  to one for  $x > 0$ .

The following scaling is used: unit time is taken to be the oscillation period,  $T_0$ , of the FHN kinetics. The value of  $\gamma$  is then set equal to  $T_0$  such that eqn. (6) oscillates with a period  $T' = 1$  at  $x = 0$ . For instance, the oscillation period of the FHN kinetics is  $T_0 = 1.79988$  when  $w = 0$ ,  $\varepsilon = 10$ ,  $\alpha = 2$ ,  $\gamma = 1$  and by setting  $\gamma = T_0$  the oscillation period becomes one. This scaling is implicitly assumed in all simulations in the subsequent sections. Unit length,  $l$ , is chosen such that the re-scaled flow velocity is  $\phi T'/l = 1$ . This corresponds to an axial extension of one somite length for each completed posterior oscillation. With this choice of space- and timescales, the diffusion coefficients are re-scaled by a factor equal to  $T'/l^2$ . In all the simulations, we take  $\varepsilon_w = 1$ ,  $p = 1$  and  $w_0 = 5 \times 10^{-5}$ . The FHN kinetics is symmetric, *i.e.*  $\beta = 0$ , unless otherwise stated.

### 3.3 Phase-wave scenario

The first scheme is a RDA version of our earlier phase-mode.<sup>22</sup> It involves an oscillation period that approaches infinity as the cell age increases. As  $w(a)$  increases from  $w_0$  at  $x = 0$  towards a value of one far from it, the value of  $R$  (see Section 2.1) is made to change from one to zero by setting  $\gamma(a) = T_0[1 - w(a)]$ . The diffusion coefficients are equal.

The simulations in Fig. 7 shows the spatio-temporal phase dynamics at different values of the diffusion coefficients. It is observed, that each boundary oscillation induces a wave that travels in the anterior direction with decreasing width and velocity, in agreement with the experimentally recorded wave behaviour. When the diffusion coefficients are low, the gradual arrest of the oscillation gives rise to a long-lived space-periodic structure, as shown in Fig. 7(a) for  $D = 0.001$ . As demonstrated in Fig. 7(b), the lifetime of the structure is decreased when the diffusion coefficient is increased, as expected. If diffusion is too high the phase waves are dispersed before the FDS with velocity  $c = \phi$  is established. This is illustrated in Fig. 7(c).

While the relevant structure with velocity  $c = \phi$  is transient for  $D \neq 0$ , it may still be sufficiently long-lived to induce cell differentiation. Expression of segmental-clock genes is in the chick

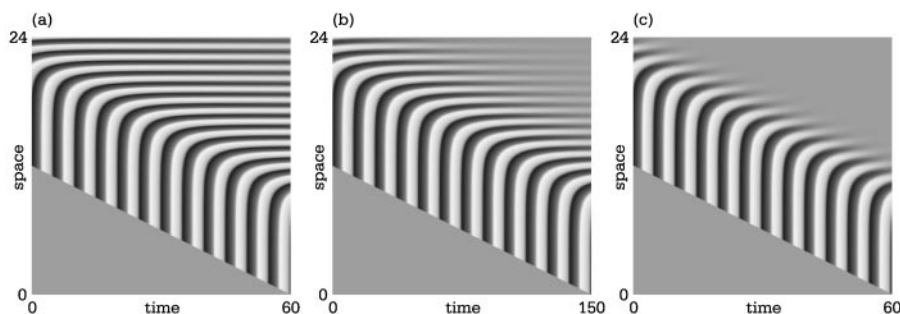


**Fig. 7** Spatio-temporal phase dynamics in the presence of diffusion. Note that the space–time plot is shown in the reference frame where the boundary moves downward. (a) A long-lived structure for  $D = 0.001$ . (b) A transient phase wave for  $D = 0.01$ . (c) The relevant structure fails to establish for  $D = 0.1$ . In all simulations:  $\gamma(a) = T_0[1 - w(a)]$ ,  $\varepsilon = 10$ ,  $\alpha = 2$ .

observed to last for at least 15 h within the mature somite,<sup>38</sup> which may be sufficient time to activate genes that are involved in cell differentiation.

The simulations in Fig. 7 shows that the diffusion coefficient must thus be lower than 0.1 for a stationary transient pattern to arise. In the chick embryo, unit time is equal to about 90 min while unit length is roughly 120  $\mu\text{m}$ . Assuming that the FHN kinetics gives a reasonable approximation to the real gene expression cycle, that is, with dimensional-dependent variables and dimensionless dynamic variables, the diffusion coefficients within the chick embryo must be less than about  $10^{-9} \text{ cm}^2 \text{ s}^{-1}$ . This value is quite low (by a factor of 100) compared to diffusion coefficients of macromolecules in water. It is not unrealistically low, however, since the molecules may be embedded in the cell membrane or confined to the interior of the cells. Then it is the Brownian motion of the cells that leads to dispersion of the pattern, not the Fickian diffusion of molecules in water.

### 3.4 Turing scenario

Based on the investigation in Section 2.2, it is expected that the relevant Turing-type FDS arises in a regulatory scheme where  $\varepsilon$  gradually decreases as cells age. This is verified by the simulation presented in Fig. 8(a) where  $\varepsilon$  depends on cell age through  $\varepsilon(a) = 9.05[1 - w(a)] + 0.95$ . Hence,  $\varepsilon$  is equal to 10 (oscillatory local kinetics) near the boundary and decreases to a value of 0.95 as cells move downstream. This corresponds to a slow passage through the supercritical Hopf bifurcation at  $\varepsilon = 1$ . The homogeneous state is made Turing-unstable by increasing the diffusion coefficient of the inhibitor.

The situation in Fig. 8(a) is a bit more complicated than that investigated in Section 2.2 since a Turing-type FDS is supported for the parameter values in the boundary region. However, it does not spontaneously replace the homogenous oscillation. As  $\varepsilon(a)$  decreases, the increasing oscillation period establishes the beginning of a space-periodic pattern and the homogenous oscillation is converted into a Turing-type FDS. This occurs before  $\varepsilon$  passes through the Hopf bifurcation of the local kinetics. Hence, the local steady state needs not to become stable for a space-periodic pattern to be formed. This is illustrated in Fig. 8(b) where the decrease in  $\varepsilon$  stops short of the Hopf bifurcation.

The slowed-down oscillation used in the phase-wave scenario may also be replaced by a Turing-type FDS in the presence of a long-ranged inhibitor. Hence, it is not required that the local kinetics is arrested, *i.e.*  $T_0 \rightarrow 0$ , as assumed in Section 3.2. Suppose that the period of the intrinsic oscillation is increased through a decrease in  $\gamma$ , but that it does not decrease to zero. In the absence of differential diffusion, the result would be travelling waves whose velocities are greater than the flow velocity. However, the presence of a long-ranged inhibitor may cause arrest of oscillation,  $T = \infty$ , without the arrest of the local kinetics,  $T_0 = \infty$ . This scenario is illustrated in the space-time plot in Fig. 8(c).

Both the phase-wave and the Turing schemes reproduce the spatio-temporal behaviour of the gene expression waves quite well. Based on the space-time plots, it is not possible to determine which one is more likely to be operating during somitogenesis. However, a Turing-type FDS will

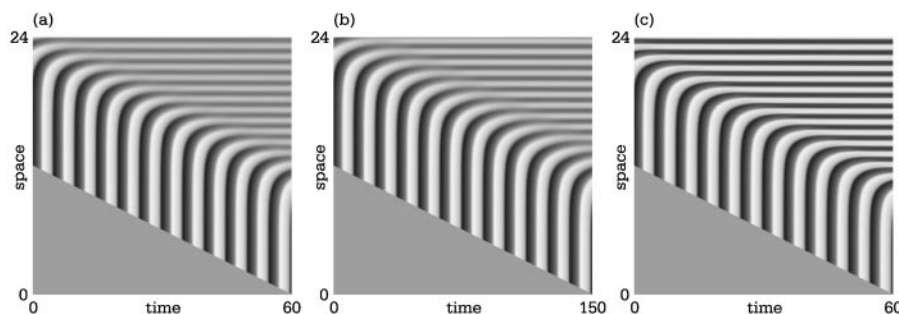


**Fig. 8** Spatio-temporal behaviour in Turing-unstable media. (a) The activator kinetics is gradually slowed down:  $\varepsilon(a) = 9.05[1 - w(a)] + 0.95$ . (b) Passage through the Hopf-bifurcation does not occur:  $\varepsilon(a) = 8.5[1 - w(a)] + 1.5$ . (c) Arrest of oscillation caused by differential diffusion:  $\gamma(a) = T_0[1 - 0.8w(a)]$ . In all simulations:  $D_u = 0.01$ ,  $D_v = 0.1$ . Other parameter values are given in Fig. 7.

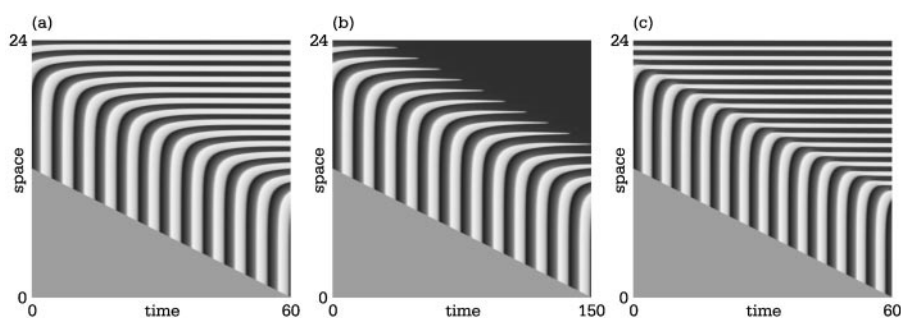


**Fig. 9** Spatio-temporal behaviour in bistable media for  $\varepsilon = 10$ . (a) Persistent structures with equally stable states:  $\alpha(a) = 2[1 - w(a)]$ ,  $\beta = 0$ ,  $D_u = D_v = 0.01$  (b) The low activator state absorbs the high activator state:  $\alpha(a) = 1.7[1 - w(a)] + 0.3$ ,  $\beta = 0.05$ ,  $D_u = D_v = 0.01$  (c) Persistent structures when the inhibitor diffusion coefficient is increased to  $D_v = 0.2$  with the other parameters as in (b).

spread spatially. Recent experiments on *zebrafish* by Jiang *et al.*<sup>44</sup> indicate that stable stripes may coexist with tissue that contains no stripes. The authors interpret the experimental observations as arising from the de-phasing of the posterior synchronous oscillation. This interpretation implies that cells after a while enter the PSM with random phases. One would then expect a noise-sustained Turing-type FDS under convectively unstable conditions, and a space-filling Turing-type FDS under absolutely unstable conditions (see Section 2.2). Since this is not what is observed, a Turing-like mechanism is probably not involved in the regulation of the gene expression in *zebrafish*. The phase-wave scenario on the other hand produces a number of stripes while the posterior oscillation is coherent and no stripes when it has desynchronized.

### 3.5 Interface scenario

The FHN kinetics in eqn. (9) is bistable when  $\alpha < 2/3$  and  $\beta = 0$ . When  $\alpha$  is equal to zero, the inhibitor is independent of the activator and converges rapidly to the stable steady state given by  $v = \beta$ . For  $\beta = 0$ , the states with high and low activator levels have the same relative stability and interfaces with velocity  $c = \phi$  are supported. An example of persistent FDS that arise for equal diffusion coefficients when  $\alpha(a) = 2[1 - w(a)]$  is shown in Fig. 9(a). There is no qualitative difference between the interface-type FDS and those observed in Fig. 7 (phase-wave FDS) and in Fig. 8 (Turing-type FDS).

If  $\beta$  is greater than zero, the state with low activator state is more stable than the high activator state. The space-time plot obtained when  $\beta$  is 0.05 and the value of  $\alpha$  changes according to  $\alpha(a) = 1.7[1 - w(a)] + 0.3$  is shown in Fig. 9(b). The diffusion coefficients are equal and the state with high activator levels is gradually absorbed by the state with low activator levels. However, increasing the diffusion coefficient, *i.e.* adding long-range inhibition, allows for the formation of persistent interface-type FDS, as in Section 2.3. The space-time plot shown in Fig. 9(c) is obtained from a simulation where the parameters are the same as in Fig. 9(b), with the exception that the ratio of inhibitor and activator diffusion coefficients is 10 : 1.

FDS of the interface-type typically consist of localised and self-sustained elements that do not spread spatially. The homogeneous state is stable and stripes may form only in one part of the PSM. If the coherence of the boundary oscillation is gradually lost (as in the interpretation by Jiang *et al.* mentioned above), a number of stripes would be formed early in somitogenesis. None would however form at a later stage when the boundary synchronisation has deteriorated.

## 4 Discussion

The spatio-temporal dynamics of open flow systems is often dictated by the temporal dynamics at the origin of the flow, *i.e.* at the inflow boundary. Given appropriate conditions, the boundary dynamics imposes itself onto the system as a whole and forces it into a variety of space-periodic wave-patterns. This is the result of the flow,  $\phi$ , converting a temporal boundary-periodicity,  $T'$ , into a spatial periodicity,  $\phi T'$ . The boundary-imposed spatial mode can be modified or maintained by the intrinsic kinetics of the flowing medium. For instance, boundary forcing of flows of

oscillatory media can result in upstream and downstream travelling waves whose wavelengths are different from the imposed periodicity. The spatio-temporal dynamics is nevertheless dictated by the period of the boundary forcing (see *e.g.* ref. 18).

In this paper, we have focussed on the special but biologically relevant case where the entrainment of the dynamics leads to space-periodic wave patterns that are stationary relative to the flowing medium. They have velocities  $c = \phi$  relative to the upstream boundary and arise in periodically boundary-forced RDA systems when the local kinetics is monostable, bistable or oscillatory. The three schemes investigated involve: (1) phase waves with oscillatory local kinetics and a very long period, (2) Turing structures with monostable or oscillatory local kinetics and (3) interfacial structures with bistable or excitable local kinetics. In all three cases, the boundary-imposed spatial periodicity may be maintained, resulting in space-periodic flow-distributed structures (FDS) with velocities  $c = \phi$  and wavelengths  $\lambda = \phi T'$ .

The entrainment of dynamics in open flows has important implications for axial segmentation in biology. We have shown how axial growth in developing organisms is equivalent to an open flow. It is not important whether a “real” flow is actually present since the open flow concept applies to all system where there is a relative motion between elements and an upstream boundary. The flow may for instance arise from proliferation of stem cells within a TGZ, as is observed in many annelids, arthropods and plants and in some cases of limb development. The progeny cells remain fairly stationary relative to the embryo as a whole and the open flow arises as the distance between a cell and the TGZ increases in time. Alternatively, cells from the surrounding tissue may be recruited to a growth zone at the tip of an elongating structure. The early development of birds and mammals, for example, is known to involve such an organising centre located prior to the axially growing PSM.

We have demonstrated how the operation of an oscillator (a segmental clock) that is synchronised at the growth boundary gives rise to space-periodic variation in a morphogen level along the growth-axis of the developing embryo. The involvement of axial growth and a segmental clock in the formation of space-periodic stripes of gene expression has been demonstrated experimentally during somitogenesis in fish, birds and mammals. The stripes become stationary relative to cells at the anterior end of the PSM, just before a somite is formed.<sup>37</sup> The wavelength of the gene expression wave is observed to be equal to  $\lambda = \phi T'$ , which provides evidence that it is imposed by the combination of a growth-induced flow and an oscillation that is synchronised at the growth boundary.

While the above described scenarios relate to somitogenesis in vertebrates, the axial segmentation observed in many invertebrates is also consistent with the formation of FDS. It is well established that during the development of the intermediate germ-band insect *Tribolium*, stripes of gene expression appear one after the other at a short distance from a TGZ of proliferating stem cells. However, gene expression waves have not been experimentally recorded for sequential segmentation in annelids and arthropods, but this may be attributed to a lack of research so far directed towards recording spatio-temporal sequences of gene expression.<sup>45</sup> The key issue, namely whether a synchronised oscillation is present within the TGZ has yet to be investigated.

Another important prediction is that an organism can achieve a global control of its developmental dynamics by regulating the rate of axial growth,  $\phi$ , and the period of the segmental clock,  $T'$ . For instance, if the shedding of progeny cells from a stem cell population facilitates axial growth, the rate of growth would be proportional to the number of stem cells. By microsurgery, Cooke<sup>46</sup> reduced the number of cells residing at the terminal end of the developing frog embryo. He observed that the number of somites remained the same, but that they were reduced in size. This is consistent with our prediction that the wavelength,  $\lambda = \phi T'$ , is decreased when the growth rate is reduced by lowering the number of feeding stem cells. In addition, it seems logical that the number of feeding stem cells scales linearly with the overall size of the embryo. In this case, our prediction accounts for size adaptation: a small embryo would naturally produce that same number of segments as a large embryo, but the size of the segments would scale proportionally to the overall size of embryo.

Which one of the scenarios is actually operating may be difficult to determine experimentally since they give rise to the same qualitative wave behaviour. In an evolutionary context, this allows for the transformation from one scenario into another. Consider a biological system that forms stripes due to an age-dependent arrest of the segmental clock. Strong cell–cell signalling (modelled

here as a diffusive process) causes the stationary stripes to become transient and may prevent their formation altogether. However, strong coupling spatial couplings (*i.e.* high  $D_u$  and  $D_v$ ) near the growth zone is allowed and could, for instance, ensure that boundary oscillation be properly synchronised among cells. A mutation that substantially reduces the activator signalling (*i.e.*  $D_u$ ) could then result in stripe formation by a different mechanism, namely the Turing-type FDS. The organism may survive since the wavelength of stationary pattern,  $\lambda = \phi T'$ , may be the same before and after the mutation. Alternatively, an ancient species could have survived a series of mutations that gradually increases the mobility of the inhibitor (*e.g.* a cell-signalling molecule) while the mobility of the activator (*e.g.* a cell-internal factor) is kept low. In the same vein, mutations from a periodically forced oscillating medium to a bistable medium may result in viable embryos with the same resulting stationary pattern.

The scenarios that involve FDS of the phase wave and the Turing type are closely related to other models of biological morphogenesis. For instance, a number of current models of somitogenesis (see discussion in ref. 22) implicitly or explicitly involve phase dynamics. However, only the recent clock-and-trail model by Kerszberg and Wolpert<sup>47</sup> explicitly considers that axial growth combined with an oscillation at the posterior boundary may entrain the developmental dynamics. The authors suggest that the stem cells feeding the growing structure oscillate in synchrony and that daughter cells preserve a “snapshot” of the oscillation phase. This model corresponds to periodic boundary forcing of a medium whose local kinetics has an infinite period of oscillation (*i.e.*  $R = 0$ ). Our earlier phase model<sup>22</sup> involved the same principle, but with a value of  $R$  that decreases gradually from one to zero as cells age. Indeed, the phase-wave scenario without cell-cell communication (diffusion) accounts well for the experimentally observed spatio-temporal behaviour of gene expression waves and can be made consistent with a large number of other experimental observations (see ref. 22 for details).

To preserve the cell-intrinsic regulation of the segmental clock in the chick, we assumed in Section 3 that its kinetics, through  $w(a)$ , depends only on the time,  $a$ , that a cell has spent in the PSM. However, the regulation of the segmental clock could involve cell-external factors and  $w$  could, for instance, represent the level of a cell-signalling molecule. The regulation of  $w$  in eqn. (11) may readily be adapted to model this situation because it allows a propagation front-solution. Suppose that the system initially is in the  $w = 0$  steady state and that the flow is absent. A front connecting the steady states at  $w = 0$  and  $w = 1$  may develop if a perturbation in  $w$  is applied locally. For  $p = 1$  it propagates at a velocity  $c_0 = 2\sqrt{\varepsilon_w D_w}$ .<sup>42</sup> If the local kinetics depends on the level of  $w$ , this would lead to sequential segmentation along the body-axis if the front propagates from the anterior towards the posterior end of the embryo. The wavelength would be given by  $\lambda = c_0 T'$ , where  $T'$  is the oscillation period ahead of the front. This scenario corresponds to the classic clock and wave front model by Cooke and Zeeman,<sup>48</sup> which may very well account for sequential segmentation in the absence of growth, as observed, for instance, during the early stages of amphibian somitogenesis.

The involvement of an independent wave front seems however unlikely in species where the growth zone and the segments are separated by an unsegmented tissue of constant length, such as the PSM in many vertebrates. This would require that the front velocity,  $c_0$ , be linked to the growth rate,  $\phi$ , since a constant length of the unsegmented tissue can arise only if  $c_0 = \phi$ . This is also required to give the wavelength  $\lambda = \phi T'$  observed during somitogenesis in the chick.

For the same reason, a mechanism where a space-periodic structure is formed by the spreading of an intrinsically selected (*i.e.* Turing-like) structure would require that the velocity of the spreading structure, also denoted by  $c_0$ , be coupled to the rate of growth. As pointed out by Meinhardt,<sup>2</sup> such a mechanism may be operational in axially growing systems where segments arise close to the growth boundary and in non-growing systems where segments arise sequentially. In the former case, the relevant Turing-type FDS arises when  $c_0 > \phi$  or as noise-sustained structure when  $c_0 < \phi$ . A segmental clock at the boundary is therefore not necessary. However, its presence would seem advantageous as it allows a more flexible control of the developmental dynamics.

In contrast to phase waves and Turing structures, bistable local kinetics is not commonly found in models of biological morphogenesis. This is probably because a medium with bistable local kinetics does not develop space-periodic structures spontaneously. In reaction-diffusion systems, one of the stable homogeneous steady states is typically selected. The operation of a segmental clock at the TGZ may however induce a space-periodic pattern if it periodically switches between

the basins of attraction of the stable steady states. The result is actually one of the most robust ways to produce persistent FDS. Any wavelength above a critical wavelength can be imposed and a long-ranged inhibitor is not required if the two steady states have the same relative stability. In this context, it is worth noting that the view of cell differentiation as a dynamic process involving multiple steady-state attractors is gaining momentum (see *e.g.* ref. 49). It is possible that the purpose of the waves produced by the segmental clock is to determine the fate of cells by switching between the basins of attraction of steady states in a cell regulatory network. A particular cell state would then be induced once the waves have become stationary relative to cells. A switch that determines cell fate and is influenced by segmental clock genes was recently demonstrated in mouse somitogenesis.<sup>50,51</sup>

In summary, we have demonstrated how the combination of axial growth and periodic boundary forcing robustly gives rise to space-periodic structures in developing embryos. All that is required to produce these waves is:

- (1) An open flow established by axial growth.
- (2) A segmental clock that is synchronised at the growth boundary, and
- (3) Means for maintaining the boundary-imposed periodicity.

We have described three generic scenarios for the formation of waves in boundary-forced open flows of active media and discussed their relevance to axial segmentation. They involve local kinetics and spatial interactions that are feasible in chemical systems and represents therefore some of the simplest mechanisms to achieve self-organisation in biology.

## References

- 1 A. M. Turing, *Philos. Trans. R. Soc. London, Ser. B*, 1952, **237**, 37.
- 2 H. Meinhardt, *Models of Biological Pattern Formation*, Academic Press, New York, 1982.
- 3 V. Castets, E. Dulos, J. Boissonade and P. DeKepper, *Phys. Rev. Lett.*, 1990, **64**, 2953.
- 4 Q. Ouyang and H. L. Swinney, *Nature*, 1991, **352**, 612.
- 5 J. E. Pearson, *Science*, 1993, **261**, 189.
- 6 K. J. Lee, W. D. McCormick, J. E. Pearson and H. L. Swinney, *Nature*, 1994, **369**, 215.
- 7 J. Boissonade, *Nature*, 1994, **369**, 188.
- 8 S. Kondo and R. Asai, *Nature*, 1995, **376**, 765.
- 9 P. K. Maini, K. J. Painter and H. N. P. Chau, *J. Chem. Soc., Faraday Trans.*, 1997, **93**, 3601.
- 10 A. Hunding, in *On Growth and Form*, ed. M. A. J. Chaplain, G. D. Singh and J. C. McLachlan, Wiley, New York, 1999, pp. 75–88.
- 11 R. Satnoianu, M. Menzinger and P. K. Maini, *J. Math. Biol.*, 2000, **41**, 493.
- 12 R. J. Deissler, *J. Stat. Phys.*, 1985, **40**, 371.
- 13 V. Z. Yakhnin, A. B. Rovinsky and M. Menzinger, *Can. J. Chem. Eng.*, 1995, **74**, 647.
- 14 S. P. Kuznetsov, E. Mosekilde, G. Dewel and P. Borckmans, *J. Chem. Phys.*, 1997, **106**, 7609.
- 15 R. Satnoianu, J. H. Merkin and S. K. Scott, *Physica D*, 1998, **124**, 345.
- 16 P. Andrésén, M. Bache, E. Mosekilde, G. Dewel and P. Borckmans, *Phys. Rev. E*, 1999, **60**, 297.
- 17 M. Kærn and M. Menzinger, *Phys. Rev. E*, 1999, **60**, 3471.
- 18 M. Kærn and M. Menzinger, *Phys. Rev. E*, 2000, **61**, 3335.
- 19 R. Satnoianu and M. Menzinger, *Phys. Rev. E*, 2000, **62**, 113.
- 20 R. Satnoianu, J. H. Merkin and S. K. Scott, *Dyn. Sys. Appl.*, 1999, **14**, 275.
- 21 M. Kærn, M. Menzinger and A. Hunding, *Biophys. Chem.*, 2000, **87**, 121.
- 22 M. Kærn, M. Menzinger and A. Hunding, *J. Theor. Biol.*, 2000, **207**, 473.
- 23 M. Kærn and M. Menzinger, *Phys. Rev. E*, 2000, **62**, 2994.
- 24 A. Hunding and M. Brøns, *Physica D*, 1990, **44**, 285.
- 25 J. G. Blom and P. A. Zegeling, *Trans. Math. Software*, 1994, **20**, 197.
- 26 M. T. M. Koper, *J. Chem. Phys.*, 1994, **102**, 5278.
- 27 S. P. Dawson, M. V. D'Angelo and J. E. Pearson, *Phys. Lett. A*, 2000, **265**, 346.
- 28 A. Hunding and R. Engelhardt, *J. Theor. Biol.*, 1995, **173**, 401.
- 29 J. H. Merkin, R. Satnoianu and S. K. Scott, *Dyn. Sys. Appl.*, 2000, **15**, 209.
- 30 A. Hagberg and E. Meron, *Nonlinearity*, 1994, **7**, 805.
- 31 A. Hagberg, E. Meron and T. Passot, *Phys. Rev. E*, 2000, **61**, 6471.
- 32 A. S. Mikhailov, *Foundations of Synergetics I*, Springer-Verlag, New York, 1990.
- 33 J. M. Chomaz, *Phys. Rev. Lett.*, 1992, **69**, 1931.
- 34 P. L. Tam, D. Goldman, A. Camus and G. C. Schoenwolf, *Curr. Top. Dev. Biol.*, 2000, **47**, 1.
- 35 K. J. Dale and O. Pourquié, *Bioessays*, 2000, **22**, 72.
- 36 C. D. Stern and D. Vasiliaskas, *Curr. Top. Dev. Biol.*, 2000, **47**, 107.
- 37 C. D. Stern, S. E. Frase, R. J. Keynes and D. R. N. Primmitt, *Development*, 1988, **104**, 231.

- 38 I. Palmeirim, D. Henrique, D. Ish-Horowicz and O. Pourquié, *Cell*, 1997, **91**, 639.
- 39 Y. Jiang, L. Smithers and J. Lewis, *Curr. Biol.*, 1998, **8**, 868.
- 40 I. D. Barrantes, A. J. Elia, K. Wünsch, M. Hrabê de Angelis, W. T. Mak, J. Rossant, R. A. Conlon, A. Gossler and J. L. de la Pompa, *Curr. Biol.*, 1999, **9**, 470.
- 41 O. Pourquié, *Curr. Top. Dev. Biol.*, 2000, **47**, 81.
- 42 J. D. Murray, *Mathematical Biology*, Springer-Verlag, New York, 2nd edn., 1993.
- 43 J. E. Ferrell, *Trends Biochem. Sci.*, 1997, **22**, 288.
- 44 Y. J. Jiang, B. L. Aerne, L. Smithers, C. H. C. D. Ish-Horowicz and J. Lewis, *Nature*, 2000, **408**, 475.
- 45 W. G. M. Damen, M. Weller and D. Tautz, *Proc. Nat. Acad. Sci. USA*, 2000, **97**, 4515.
- 46 J. Cooke, *Nature*, 1975, **254**, 196.
- 47 M. Kerszberg and L. Wolpert, *J. Theor. Biol.*, 2000, **205**, 505.
- 48 J. Cooke and E. C. Zeeman, *J. Theor. Biol.*, 1976, **58**, 455.
- 49 S. Huang and D. E. Ingber, *Exp. Cell Res.*, 2000, **261**, 91.
- 50 Y. Takahashi, K. Koizumi, A. Takagi, S. Kitajima, T. Inoue, H. Koseki and Y. Saga, *Nature Genet.*, 2000, **25**, 390.
- 51 C. D. Stern, *Nature Genet.*, 2000, **25**, 368.